

## RESEARCH OF DYNAMIC PROCESSES IN AN ANVIL DURING A COLLISION WITH A SAMPLE

Yuriy PYR'YEV<sup>\*✉</sup>, Andrzej PENKUL<sup>\*\*✉</sup>, Leszek CYBULA<sup>\*\*✉</sup>

\*Faculty of Mechanical and Industrial Engineering, Institute of Mechanics and Printing, Department of Printing Technologies, Warsaw University of Technology, ul. Konwiktorska 2, 00-217 Warsaw, Poland

\*\*Faculty of Mechanical and Industrial Engineering, Institute of Mechanics and Printing, Department of Mechanics and Weaponry Technology, Warsaw University of Technology, ul. Narbutta 85, 02-524 Warsaw, Poland

[yuriy.pyr'yev@pw.edu.pl](mailto:yuriy.pyr'yev@pw.edu.pl), [andrzej.penkul@pw.edu.pl](mailto:andrzej.penkul@pw.edu.pl), [leszek.cybula@pw.edu.pl](mailto:leszek.cybula@pw.edu.pl)

received 3 October 2022, revised 15 December 2022, accepted 18 December 2022

**Abstract:** The paper concerns modelling the dynamics of the contact system of the tested sample with an elastic half-space (anvil) during their collision. The original elements in the paper include the proposed general approach to solving the problem of contact dynamics. The presented approach consists in determining the force of impact on the sample during the collision and the joint solution of the problem for the tested sample and the problem for an elastic semi-space under the conditions of the assumptions of Hertz's theory. The resulting interaction forces allow the determination of displacements and stresses.

**Keywords:** collision, test sample, anvil, half-space, elastic waves, impact speed, Hertz's theory

### 1. INTRODUCTION

The purpose of the paper is to analyse the wave phenomena occurring during the impact of the test sample against the anvil (elastic half-space) and to develop a method for calculating the parameters of selected physical quantities occurring in the anvil and the sample (projectile [1]) in the initial period after the impact.

Experimental database used as input (comparative) data were the impact tests of the Taylor bar. The impact test was proposed by Taylor [1], Whiffin [2] and Carrington and Gayler [3] as an experimental method of measuring the dynamic yield strength  $R_{yd}$  of elastic-plastic materials [1–3].

Many examples of shock-type transient processes with high strain rates can be found in the field of artillery [4–7] and in the study of seismology, earthquake engineering, dynamic soil-substrate interaction and terrain characteristics, and in mathematical modelling of the erosion process.

The problem of collision of elastic bodies with regard to their deformation has a rich history. The elementary collision theory uses the restitution factor  $R_f$  as a key parameter characterizing the deformation properties of colliding bodies and does not reflect various features of the internal state of the bodies [8, 9].

Saint-Venant [10], considering the propagation of longitudinal waves, considered the axial impact of the rods. It turned out that the theoretically determined time of collision differs significantly from the time obtained during the experiment. The reason for these differences is the inability to ensure the perfect flatness of the rod ends.

Hertz [11], based on Boussinesq's [12] research on the deformation of an elastic half-space, solved the problem of direct central collision of spheres with elastic properties, considering only local static deformations (ignoring wave propagation). In this case, the agreement between the theoretical and experimental

collision times turned out to be good. Hertz's theory of impacts is used in practice to determine the stresses during interactions of two bodies with each other [13].

Sears [14] combined the Saint-Venant and Hertz approaches and considered the influence of the spherical shape of the rod ends on the obtained results. In these studies, he took into account both local deformations and wave propagation. This approach led to a good agreement of theoretical and experimental results and is used in many subsequent works [15, 16].

Kil'chevskii [8] modified Hertz's theory by combining it with Saint-Venant's theory.

The theory of crossbeam impact comes from Timoshenko et al. [17].

The problem concerning the phenomena occurring in an elastic semi-space hit by a moving mass on the surface has been investigated, e.g., in articles [18–24].

Kubenko [19] presented an overview of the approaches to study the impact of a blunted elastic body on the surface of an elastic medium. Mathematically, the problem is generally formulated as the non-stationary mixed boundary problem of continuum mechanics in which the unknown contact boundary changes with time and space.

The collision process between a blunted body and an elastic medium always includes a supersonic stage, during which the boundary value problem can be formulated as non-mixed and thus solved with simpler methods [19, 20].

In the paper [21], the problem of the linear theory of elasticity concerning the response of the elastic surface of the half-space to the normal impact of the indenter was considered.

In the paper [22], an exact analytical solution of the problem was obtained for the impact of a rigid mass on a semi-infinite elastic rod by a Kelvin-Voigt linear element.

The impact of the super seismic phase on the collision process immediately after the first contact is investigated within the

framework of Hertz's theory of impacts in the paper [20]. For small values of the  $\alpha A$  parameter (defined in point 4), the influence of the super seismic state on the course of the impact can be neglected.

Ruta and Szydło [25] presented a method enabling the conversion of the results of the dynamic weight test into a static model. This paper presents an analytical solution to the problem of half-space vibrations caused by the shock pulse.

In the paper [26], the ground was modelled as an idealised elastodynamic half-space, and its sound emission during the collision of the object with the ground was analysed.

Since the classic work of Lamb [27] on the transient elastic response of a half-space resulting from the sudden application of a normal surface line and point loads, significant progress has been made in solving this class of elastodynamic problems [28].

Beginning with the ground-breaking work [27], Lamb's problem, which relates to the dynamic response on the free surface of an elastic half-space resulting from a time-dependent point pulse on a free surface, has become a classic subject of numerous theoretical seismology studies. Cagniard [29] presented a complicated method using the Laplace transform over time and presented the final solutions in the time domain. Thanks to the modification made by de Hoop [30], it became an appropriate way to solve the Lamb problem, which is now referred to as the 'Cagniard-de Hoop method'. The problem was taken up again by Sánchez-Sesma et al. [31] who provided a full set of formulas with an exact solution for any source and recipient location. Pak and Bai [32] presented an improved but compact analytical formula of the elastodynamic response in the time domain of a three-dimensional half-space subjected to an arbitrary distribution of internal or surface forces. For a surface point pulse operating on a 3D medium, Pekeris [33] gave a closed solution for a vertical point source, and Mooney [28] extended the results for vertical loads by any Poisson's ratio, ignoring the radial component.

Kausel [34, 35] dealt with the problem of Lamb applied to the soil, horizontal and vertical point load applied to the surface of an elastic, homogeneous half-space with any Poisson's ratio. A compact set of unambiguous space time formulas was presented for the following problems: all response functions for receivers placed on the surface of the half-space and at the depth under the load, i.e., along the epicentral axis.

Emami and Eskandari-Ghadi [36] presented a history of this problem, from its earlier stages to more recent research, by outlining and discussing the various rigorous approaches and methods of solving that have been suggested so far.

We shall consider the collision of elastic bodies (Figs. 1 and 2). The study will be conducted with the basic geometric assumptions of Hertz's theory [11].

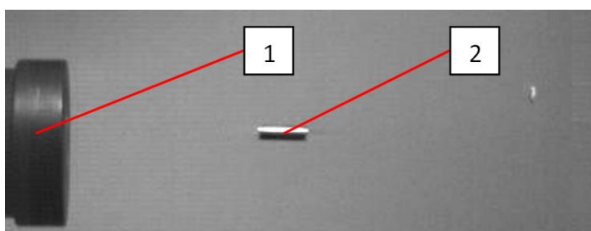


Fig. 1. View of the sample on the flight path before hitting the anvil: (1) anvil and (2) research sample

We limit ourselves to considering the direct interaction of the central bodies, i.e., we assume that they are the resultant of the

dynamic contact pressures applied to the colliding bodies, directed along a straight line connecting their centres of inertia and coinciding with the normal to the compression surface at the point of initial contact of the non-deformed surface of these bodies.



Fig. 2. The sample at the moment it hits the anvil

This simplifying assumption will allow us to take into account only one component of the displacements of bodies at the point coinciding with the point of their initial contact.

## 2. IMPACT PROBLEM STATEMENT

Let us assume that a heavy body hits the half-space and has  $V_0$  velocity when it contacts the surface of the half-space. Under the influence of an impact in a half-space and in a striking sample of  $r_0$  radius, local deformations will be created, and, additionally, vibrations of the half-space will arise. Let us assume that the friction between the contacting surfaces is negligible, and the material of the elastic space with Young's modulus  $E$  and Poisson's ratio  $\nu$  does not undergo plastic deformation or fracture.

The assumption about the elastic behaviour of metal anvil (target) can be extended to the case of real processes, when only local plastic deformations occur in the material, limited by the proximity of the starting point of contact; moreover, the energy needed to create a residual indentation is only a small fraction of the initial kinetic energy [18].

By continuing the contact of the impact sample with the half-space, the displacements of the sample will consist of a part dependent on local compression and a part determined by dynamic deflections of the half-space. As is known, the dynamic deflections of the half-space satisfy the differential Eq. (1).

### 2.1. Mathematical model of the anvil

The point source causes the appearance of volumetric longitudinal (P) and shear (S) waves and Rayleigh (R) waves. Lamb [27] considered two external problems of wave propagation in an isotropic elastic half-space from a normally applied concentrated force to a free force. The solution of these problems in the paper [37] has been reduced to wave equations due to the scalar and vector potential.

We consider the anvil as an elastic half-space that is rigidly fixed in a housing that is struck by the test sample. We can consider the anvil as half-space until reflected waves do not appear.

Let us consider in a cylindrical coordinate system  $(r, \theta, z)$  a half-space  $(0 \leq z < \infty)$ , where  $r$  is radius,  $\theta$  is angle and  $z$  is coordinate, as shown in Fig. 3. The medium is assumed to be homogeneous and isotropic. Axially symmetric non-stationary loads depending on position and time act on the surface  $p(r, t)$

with relative spatial distribution  $Z(r)$  and the resultant  $P(t)$ , i.e.,  $p(r, t) = Z(r)P(t)$  in time  $t > 0$ . As a result of this action, there is a vector field of displacement in the structure  $U \equiv (u, v, w)$ , where  $u, v$  and  $w$  are the components of the displacement vector on the axis,  $r, \theta$  and  $z$ . Due to the axisymmetric stress distribution, displacements, strains and stresses will be independent of the  $\theta$  angle. We have  $U \equiv (u, 0, w)$ .

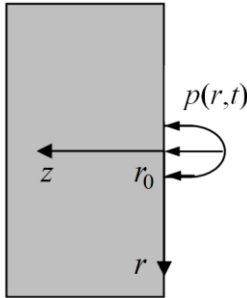


Fig. 3. Physical model of an anvil (elastic half-space) with a surface area load with  $r_0$  radius

An elastic half-space is characterised by the velocities of longitudinal (P)  $c_1$  and shear (S)  $c_2$  waves or the Lamé constants  $\lambda, \mu$  and density  $\rho$ , which are related by dependencies

$$c_1 = \sqrt{\frac{\lambda + 2\mu}{\rho}}, c_2 = \sqrt{\frac{\mu}{\rho}}$$

On the free surface of the medium, stresses  $\sigma_{zr}, \sigma_{z\theta}$  and  $\sigma_{zz}$  are either converted to zero or take values corresponding to a given limit load.

We assume that the medium is at rest when  $t < 0$ , and in the initial moment,  $t = 0$ , where the axisymmetric source of disturbances starts to work  $p(r, t) = Z(r)P(t)$ .

As a rule, the forces arising during an impact  $P(t)$  (impact force, life force) are not known in advance; they must be determined in the problem-solving process, and only in some cases can they be considered predetermined.

The discussed issue boils down to solving Lamé displacement equations in a cylindrical coordinate system [38]:

$$\begin{aligned} (\lambda + 2\mu) \left( \frac{\partial^2 u}{\partial r^2} + \frac{1}{r} \frac{\partial u}{\partial r} - \frac{u}{r^2} \right) + \mu \frac{\partial^2 u}{\partial z^2} + (\lambda + \mu) \frac{\partial^2 w}{\partial r \partial z} &= \rho \frac{\partial^2 u}{\partial t^2}, \\ (\lambda + \mu) \left( \frac{\partial^2 u}{\partial r \partial z} + \frac{1}{r} \frac{\partial u}{\partial r} \right) + \mu \left( \frac{\partial^2 w}{\partial r^2} + \frac{1}{r} \frac{\partial w}{\partial r} \right) + (\lambda + 2\mu) \frac{\partial^2 w}{\partial z^2} &= \rho \frac{\partial^2 w}{\partial t^2}, \\ 0 \leq z < \infty, 0 \leq r < \infty \end{aligned} \quad (1)$$

at boundary conditions:

$$\sigma_{zz}(r, 0, t) = -p(r, t) = -P(t)Z(r), z = 0 \quad (2)$$

$$\sigma_{rz}(r, 0, t) = 0, z = 0 \quad (3)$$

$$u, w \rightarrow 0, z \rightarrow \infty \quad (4)$$

and the initial conditions [37]:

$$u = 0, \frac{\partial u}{\partial t} = 0, w = 0, \frac{\partial w}{\partial t} = 0, t < 0 \quad (5)$$

$p(t, r)$  is the contact pressure density distributed over the contact area  $\omega(t)$ . Due to the axis of symmetry,  $\omega(t)$  is a circle with a radius  $a(t)$ . We assume that the contact area does not change with time, and from the beginning, the  $a(t)$  radius is equal to  $r_0$ .

We will consider the sources  $Z(r)$  on the surface for which the following condition is met:

$$2\pi \int_0^\infty p(r, t) r dr = P(t) \quad (6)$$

where [13]

$$Z(r) = \frac{1}{\pi r_0^2} \sqrt{1 - \frac{r^2}{r_0^2}} H\left(1 - \frac{r^2}{r_0^2}\right). \quad (7)$$

where  $H(t)$  Heaviside function:  $H(t) = 0$  for  $t < 0$ ,  $H(t) = 1$  for  $t \geq 0$ .

## 2.2. Mathematical model of a sample hitting an anvil

In the study to determine the impact of half-space, the system of equations describing the behaviour of waves in the half-space integrates simultaneously with the equation of motion of the sample and the condition of compliance of displacements. The last one takes into account a contact approximation of a sample with mass  $m_1$  and half space. One of the ends of the cylindrical rod is hemispherical. We will consider that for the considered impact of the test sample; the contact approximation can be determined on the basis of the solution to the dynamic problem of Hertz for pressing a ball into an elastic half-space [13].

Let us denote, after Timoshenko [17], the total displacement of the hitting body (projectile [1]) from the start of the impact as  $h(t)$  and local compression as  $a_H$ . Then, of course [17, 39]

$$h = a_H + w \quad (8)$$

where  $w = w(0, t)$  is deflection of the elastic semi-space surface under the sample. The displacement  $h(t)$  satisfies the differential equation of motion

$$m_1 \frac{d^2 h(t)}{dt^2} = -P(t) \quad (9)$$

under initial conditions:

$$h(0) = 0, \frac{dh}{dt} = V_0, t = 0 \quad (10)$$

Here,  $P(t)$  is the resultant of the contact pressure. In the following part, we assume that

$$\frac{m_1}{P} \frac{\partial^2 w_e}{\partial t^2} \ll 1 \quad (11)$$

where  $w_e(r, z, t)$  characterises the relative displacement of the sample elements due to its deformation.

## 3. SOLUTION METHOD

### 3.1. Key relationships for an elastic half-space

Having a solution for a concentrated force acting on a half-space boundary, the superposition method allows us to find displacements and stresses arising under the action of a load distributed in a circle [25]. This article uses a different approach [40] to find the stress-strain state of a half-space. Applying the Laplace and Hankel transformations to Eq. (1) and considering the homogeneous initial condition (5), we receive linear differential equations with respect to the variable  $z$ . Since the solution of these equations depends on four unknowns, they are found using four boundary conditions (2)–(4). By applying the inverse Laplace and Hankel transformations, we obtain the searched dependencies. Displacements  $u, w$  and stresses can be expressed by the Duhamel integral

$$\{u(r, z, t), w(r, z, t)\} = \int_0^t \{u_\delta(r, z, t-t'), w_\delta(r, z, t-t')\} \cdot P(t') dt' = \{u_\delta(r, z, t), w_\delta(r, z, t)\} * P(t) \quad (12)$$

$$\{\sigma_{zz}, \sigma_{rr}, \sigma_{\theta\theta}, \sigma_{rz}\} = \{\sigma_{zz,\delta}, \sigma_{rr,\delta}, \sigma_{\theta\theta,\delta}, \sigma_{rz,\delta}\} * P(t) \quad (13)$$

where  $u_\delta(r, z, t)$  and  $w_\delta(r, z, t)$  are solutions to problems (1)–(6) for the impulse function  $P(t) = \delta(t)$ :  $\delta(t) = \infty$  for  $t = 0$ ,  $\delta(t) = 0$  for  $t \neq 0$  and

$$\int_{-\infty}^{+\infty} \delta(t) dt = 1, \quad (14)$$

Eqs (12) and (13) give a convolution of two causal functions. Applying the Laplace and Hankel integral transformations to the considered problems (1)–(6) [37], e.g., for displacement  $w_\delta(r, z, t)$ , the equations can be written as follows:

$$w_\delta^L(r, z, s) = \int_0^\infty w_\delta(r, z, t) e^{-st} dt \quad (15)$$

$$w_\delta^{LH}(k, z, s) = \int_0^\infty w_\delta^L(r, z, s) r J_0(kr) dr \quad (16)$$

we get a solution to the problem of the following form [40]:

$$\{u_\delta, w_\delta\} = \frac{1}{2\pi i} \int_{c_0-i\infty}^{c_0+i\infty} \{u_\delta^L, w_\delta^L\} e^{st} ds \quad (17)$$

$$\{\sigma_{zz,\delta}, \sigma_{rr,\delta}, \sigma_{rz,\delta}\} = \frac{1}{2\pi i} \int_{c_0-i\infty}^{c_0+i\infty} \{\sigma_{zz,\delta}^L, \sigma_{rr,\delta}^L, \sigma_{rz,\delta}^L\} e^{st} ds \quad (18)$$

where

$$\{w_\delta^L, \sigma_{zz,\delta}^L\} = \int_0^\infty \{w_\delta^{LH}, \sigma_{zz,\delta}^{LH}\} Z^H(k) k J_0(kr) dk \quad (19)$$

$$\{u_\delta^L, \sigma_{rz,\delta}^L\} = \int_0^\infty \{u_\delta^{LH}, \sigma_{rz,\delta}^{LH}\} Z^H(k) k J_1(kr) dk \quad (20)$$

$$\sigma_{rr,\delta}^L = \int_0^\infty \sigma_{rr,\delta}^{LH0} Z^H(k) k J_0(kr) dk + \frac{1}{r} \int_0^\infty \sigma_{rr,\delta}^{LH1} Z^H(k) k J_1(kr) dk \quad (21)$$

$J_n(kr)$  is a Bessel function of the first kind of order  $n$  ( $n = 0, 1, \dots$ );  $c_0$  is a real number so that the contour path of integration is in the region of convergence of  $u_\delta^{LH}(k, z, s)$ ,  $w_\delta^{LH}(k, z, s)$ .

Integral expressions in Eqs (19)–(21) marked with 'LH' have the following form [40]:

$$u_\delta^{LH}(k, z, s) = \frac{(\gamma e^{-\alpha z} - 2\alpha\beta e^{-\beta z})k}{\mu D(k, s)} \quad (22)$$

$$w_\delta^{LH}(k, z, s) = \frac{(\gamma e^{-\alpha z} - 2k^2 e^{-\beta z})\alpha}{\mu D(k, s)} \quad (23)$$

$$\sigma_{zz,\delta}^{LH}(k, z, s) = -\frac{(\gamma^2 e^{-\alpha z} - 2\alpha\beta k^2 e^{-\beta z})}{D(k, s)} \quad (24)$$

$$\sigma_{rz,\delta}^{LH}(k, z, s) = \frac{(-e^{-\alpha z} + e^{-\beta z})2\alpha\gamma k}{D(k, s)} \quad (25)$$

$$\sigma_{rr,\delta}^{LH0}(k, z, s) = \frac{\gamma(2k^2 - (\lambda/\mu)c_1^{-2}s^2)e^{-\alpha z} - 4\alpha\beta k^2 e^{-\beta z}}{D(k, s)} \quad (26)$$

$$\sigma_{rr,\delta}^{LH1}(k, z, s) = \frac{(-2\gamma e^{-\alpha z} + 4\alpha\beta e^{-\beta z})k}{D(k, s)} \quad (27)$$

$$D(k, s) = \gamma^2 - 4\alpha\beta k^2, \gamma = 2k^2 + c_2^{-2}s^2 \quad (28)$$

$$\alpha = \sqrt{k^2 + c_1^{-2}s^2}, \beta = \sqrt{k^2 + c_2^{-2}s^2}, \text{Re}\alpha > 0, \text{Re}\beta > 0 \quad (29)$$

Hankel transform  $Z^H(k)$  of the  $Z(r)$  source on the surface Eq. (7):

$$Z^H(k) = \frac{3(\sin(r_0 k) - r_0 k \cos(r_0 k))}{2\pi r_0^3 k^3} \quad (30)$$

In order to receive the function  $w_\delta(0,0,t)$  for the initial moment  $t \rightarrow 0$ , we find the properties of the Laplace transform for  $s \rightarrow \infty$

$$w_\delta^{LH}(k, z, s) = \frac{c_2^2 e^{-\frac{zs}{c_1}}}{\mu c_1} \left( \frac{1}{s} - \frac{c_1 z k^2}{2s^2} + \dots \right) - \frac{2c_2^4 k^2 e^{-\frac{zs}{c_2}}}{\mu c_1 s^3}, s \rightarrow \infty \quad (31)$$

In the initial moment,

$$w_\delta(0,0,t) = \frac{c_2^2}{\mu c_1} H(t) Z(0), t \rightarrow 0 \quad (32)$$

$$\sigma_{zz,\delta}(0,z,t) = -\delta(t - z/c_1) Z(0), t - z/c_1 \rightarrow 0 \quad (33)$$

Asymptotics Eq. (33) shows that for the calculation of stresses, it is better to use the following equation:

$$\sigma_{zz}(r, z, t) = \int_0^t \sigma_{zz,H}(r, z, t-t') \frac{d}{dt'} P(t') dt' \quad (34)$$

where  $\sigma_{zz,H}(k, z, s) = \sigma_{zz,\delta}(k, z, s)/s$ .

$$c_2/c_1 = \sqrt{(1-2\nu)/(2-2\nu)}$$

The calculations of the inverse integral Laplace and Hankel transformations were performed in the same way as in the paper [40].

### 3.2. Solution method for the research sample

Integrating the Eq. (9) using the Laplace transform and the initial condition (10), we obtain the following equation:

$$h(t) = V_0 t - \frac{1}{m_1} \int_0^t (t-t') P(t') dt' \quad (35)$$

On the other hand, according to the theory of Hertz [13], we can assume the following equation:

$$\alpha_H = (P/K)^{2/3} = k_0 P^{2/3} \text{ or } P = K \alpha_H^{3/2} \quad (36)$$

where  $K$  is determined from the equation [13]

$$K = \frac{4E^* \sqrt{r_0}}{3}, k_0 = K^{-2/3}, \frac{1}{E^*} = \frac{1-\nu_1^2}{E_1} + \frac{1-\nu^2}{E} \quad (37)$$

Considering Eqs (8), (35) and (36), we obtain the equation:

$$V_0 t - \frac{1}{m_1} \int_0^t (t-t') P(t') dt' = k_0 P(t)^{2/3} + w(0,0,t) \quad (38)$$

At the moment of time,  $t = t_n = n\Delta t$ , where  $n = 0, 1, 2, \dots$ , where  $\Delta t$  integration time is assumed to take place

$$V_0 t_n - \frac{1}{m_1} \int_0^{t_n} (t_n - t') P(t') dt' = k_0 P(t_n)^{2/3} + w_n \quad (39)$$

where  $w_n = w(0,0,t_{n-1})$ .

In the initial moment  $t = 0$  ( $n = 0$ ), sample displacement  $h = 0$ , displacement of half-space  $w = 0$  and sample speed  $v = V_0$ .

In moment  $t = t_1$  ( $n = 1$ ), sample displacement is  $h(t_1) = h_1 = V_0 t_1$ , deflection of half-space is  $w(0,0,t_0) = w_1 = 0$ , impact force (pressure) is  $P(t_1) = P_1 = K (h_1)^{3/2}$ , acceleration of the sample is  $a_1 = -P_1/m_1$  and sample speed is  $v(t_1) = v_1 = V_0$ .

In moment  $t = t_2$  ( $n = 2$ ), sample displacement is  $h(t_2) = h_2 = h_1 + v_1 \Delta t + a_1 (\Delta t)^2/2$ , deflection of half-space is  $w(0,0,t_1) = w_2$ , impact force (pressure) is  $P(t_2) = P_2 = K (h_2 - w_2)^{3/2}$ , acceleration of the sample is  $a_2 = -P_2/m_1$  and sample speed is  $v(t_2) = v_2 = v_1 + a_1 \Delta t$ .

The further course of the calculations is obvious. Let us write directly the formulas related to the  $n^{\text{th}}$  stage:

$$h(t_n) = h_n = h_{n-1} + v_{n-1} \Delta t + a_{n-1} (\Delta t)^2/2 \quad (40)$$

$$w_n = \Delta t \sum_{m=1}^{n-2} w_\delta(0,0,t_{n-1}-t_m) P_m + \frac{\Delta t}{2} w_\delta(0,0,0) P_{n-1} \quad (41)$$

$$P(t_n) = P_n = K (h_n - w_n)^{3/2} \quad (42)$$

$$a_n = -P_n/m_1 \quad (43)$$

$$v(t_n) = v_n = v_{n-1} + a_{n-1} \Delta t \quad (44)$$

4. NUMERICAL RESULTS

A numerical analysis of the collision of a copper test sample with a steel anvil was carried out. The parameters are given in Tab. 1. The mass of the tested sample is  $m_1 = 0.0122$  kg, sample radius is  $r_0 = 0.004$  m and collision speed is  $V_0 = 100$  m/s.

Tab. 1. Mechanical properties of steel and copper

Properties	Copper	Steel
Longitudinal wave speed $c_1$ [m/s]	4,597	5,994
Shear wave speed $c_2$ [m/s]	2,263	3,204
Density $\rho$ [kg/m <sup>3</sup> ]	8,960	7,830
Coefficient $\lambda$ [GPa]	97.53	120.6
Shear modulus of elasticity $G, \mu$ [GPa]	45.9	80.4
Poisson number $\nu$ [-]	0.34	0.3
Young's module $E$ [GPa]	123	209
Yield point $R_y$ [MPa]	57	1,000
Tensile strength $R_m$ [MPa]	227	1,200

For the problem under consideration [21], the  $\alpha_A = (\pi \rho r_0^3 / m_1)^{1/2} (V_0 / c_1)^{3/2} = 0.785 \cdot 10^{-3}$  parameter was calculated. Due to the low value of  $\alpha_A$ , the influence of the super-seismic state on the course of the impact can be neglected as a whole.

Figs. 4 and 5 show the time courses of the characteristics of the test specimen during the collision. You can see that initially the force of influence on the sample  $P(t)$ , sample displacement  $h(t)$  and deflection of half-space  $w(t)$  during the collision increase and reach their maximum values. The sample speed  $v(t)$  initially drops to zero at time  $t'_s$ . The diagram of the relationship  $P(t)$  is shown in Fig. 4. Since the Hertz model describes elastic deformations, the  $P(t)$  diagram is symmetrical about the vertical axis passing through the point  $(t'_s, P_{max})$  ( $t_s = 2 t'_s$ ), where  $t_s$  is the collision time. When the force of the effect on the sample  $P(t_s) = 0$ , then  $h - w = 0$  as in Eq. (8) (Fig. 4).

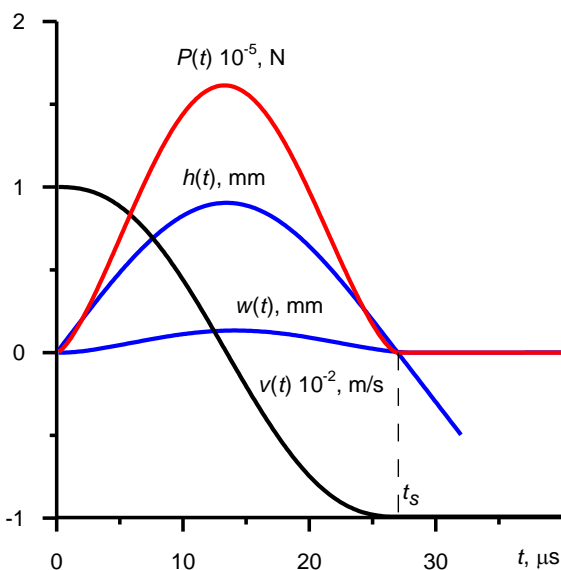


Fig. 4. Change of the force of influence on the sample  $P$ , sample displacement  $h$ , deflection of the half-space  $w$  and sample speed  $v$  over time during the Hertz impact for the collision speed  $V_0=100$  m/s

The coefficient of restitution was marked with the letter  $R_f$ . This coefficient is the ratio of the body speed after the impact  $v(t_s)$  to the speed right before the impact  $V_0$ . In the considered ranges of speeds and dimensions of colliding bodies,  $R_f = -v(t_s)/V_0 = -0.991$  ( $t_s = 27.0 \mu s$ ,  $v(t_s) = -99.1$  m/s). This factor hardly depends on these values.

Without considering the deflection of the elastic half-space, the problems (9) and (10) can be solved in the analytical form [11]. Maximum deflection can be written as follows:

$$\alpha_{max} = \left( \frac{5 m_1 V_0^2}{4 K} \right)^{2/5}, \tag{45}$$

Maximum force of impact on the sample:

$$P_{max} = K \alpha_{max}^{3/2} \tag{46}$$

Collision duration  $t_s$ :

$$t_s = 2.94 \frac{\alpha_{max}}{V_0} \tag{47}$$

This formula shows that the duration of the impact depends to the greatest extent on the mass of the sample  $m_1$  and increases with it. The duration of the collision  $t_s$  is to a lesser extent influenced by the impact speed and the reduced radius of curvature of the body contact surfaces, which is within the  $n$  factor to the 1/2 rational power. As these parameters increase, the impact time is reduced. Calculation according to Eqs (46) and (47) gives  $P_{max} = 182,191$  N and  $t_s = 24.6 \mu s$ . Calculation of the dimensionless coefficient  $K_{max} = P_{max} / S R_m = 15.97$  shows that the average maximum stresses arising in the contact area are significantly higher than the tensile strength of the sample calculated under static conditions, where for copper  $R_m = 57$  MPa and  $S = \pi r_0^2$ . Fig. 5 shows the  $K_{max}$  dependence of the radius  $r_0$  ( $K_{max} \sim 1/r_0^{9/5}$ ). Restitution coefficient is  $R_f = -1$ .

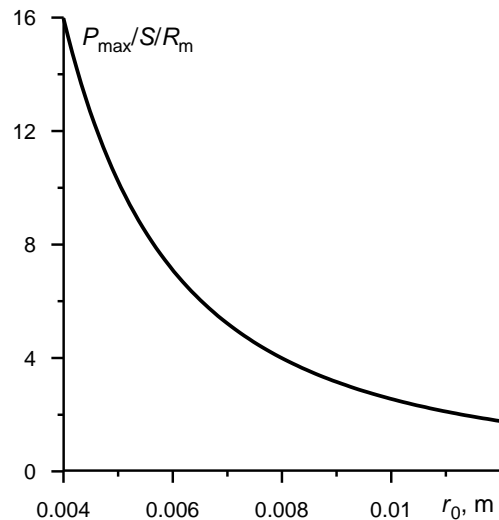


Fig. 5. The dependence of the dimensionless coefficient  $K_{max} = P_{max} / S R_m$  on  $r_0$  radius according to Eqs (46) and (45)

It was noticed in the paper [41] that the Hertz model gives results consistent with the experiment if the duration of the collision  $t_s$  is much longer than the longest period of free oscillation  $T$  of the colliding bodies,  $t_s / T > 10$ . On the other hand, according to Eq. (47), the impact duration decreases with increasing speed. Of course,

there is a certain upper limit for the speed  $V_{0,max}$ , above which the formulas obtained from Hertz's theory will lead to too considerable errors.

This consideration is often emphasised in the impact theory literature [41], but undeservedly, little attention is paid to another limitation of Hertz's theory. It is associated with the possible appearance of plastic deformations in the colliding bodies and failure to take into account the dynamic properties of strength parameters, e.g., the tensile strength parameter  $R_m$ .

If, in the post-impact conditions, the anvil was not damaged and the specimen changed shape due to plasticity (the radius of the specimen contact surface increased) but was not damaged, then the tensile strength in the specimen was not achieved. The shape of deformation and cracking in the Taylor bar impact test is the so-called mushrooming. Knowing the impact speed and the parameters of the collision bodies, we can calculate the maximum value of the force acting on the sample. This gives the opportunity to estimate the value  $R_m$ .

The dynamic yield point and the dynamic strength of the material, revealed under impact loads, assume values greater than the yield point and the material's tensile or compressive strength determined during static tests [13].

Let us note that the assumption made by Hertz about the linear elasticity of the material is not justified at sufficiently high impact velocities. Thus, Hertz's theory is probably wrong with most practical impact problems. Therefore, the work takes into account the deflection of the surface of the elastic half-space.

The performed calculations of the issue under consideration are shown in Fig. 6. We received  $P_{max} = P(t_s/2) = 160,000$  N,  $t_s = 27$   $\mu$ s and  $v(t_s) = -99.1$  m/s. In Fig. 5, the dimensionless factor was calculated,  $K_{max} = P_{max} / S/R_m = 14.11$ . Taking the deflection of the surface of the elastic half-space into account leads to an extension of the collision time and a reduction in the maximum force value  $P_{max}$  to 11.6%.

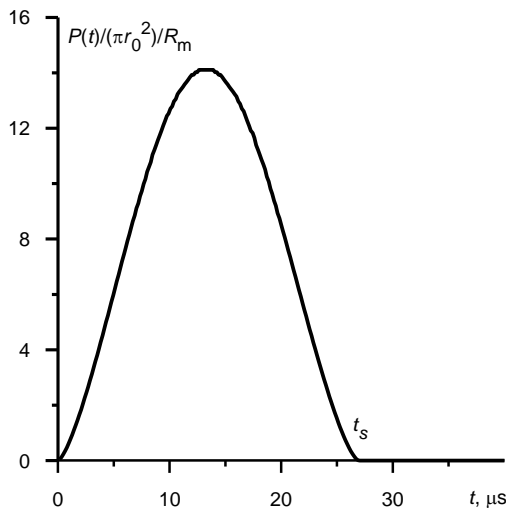


Fig. 6. Dependence of dimensionless contact stress  $P(t)/(\pi r_0^2)/R_m$  arising during the collision on time for the speed of  $V_0 = 100$  m/s

Analogously to Fig. 6, Fig. 7 shows the time dependencies of the component of vertical displacements  $w(r, 0, t)$  to the surface at four observation points. Comparing the obtained results with the displacements of the surface points from Awrejcewicz and Pyryev [40] for the disorder  $P(t)=H(t)$ , we do not observe the moment of arrival of transverse S and Rayleigh R waves. For our case, the

duration of the collision  $t_s$  is too high for the moments of arrival of longitudinal P, transverse S and Rayleigh R waves to be visible. The shape of the graphs repeats the shape of the interaction force, but away from the source, a slight negative deflection appears, the amplitude decreases and the width of the disturbance increases.

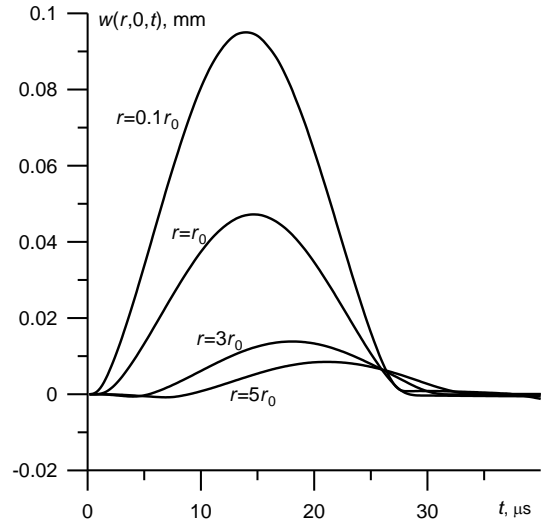


Fig. 7. Evolution of the deflection of an elastic half-space  $w(r, 0, t)$  due to load  $P(t)$  acting on the surface of a circle with a radius of the sample  $r_0$  for  $r = 0.1 r_0$  (curve 1), for  $r = r_0$  (curve 2), for  $r = 3r_0$  (curve 3) and for  $r = 5r_0$  (curve 4)

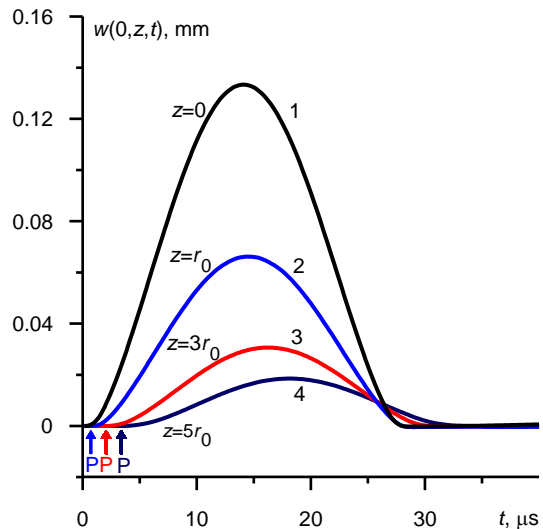


Fig. 8. Evolution of the axial displacement of an elastic half-space  $w(0, z, t)$  due to load  $P(t)$  acting on the surface of a circle with a radius of the sample  $r_0$  for  $z = 0$  (curve 1), for  $z = r_0$  (curve 2), for  $z = 3r_0$  (curve 3) and for  $z = 5r_0$  (curve 4)

Fig. 8 shows the timing of the axial displacement of the elastic half-space  $w(0, z, t)$  to load  $P(t)$  acting on the surface of a circle with a radius of the sample  $r_0$  for  $r = 0.1 r_0$  (curve 1), for  $r = r_0$  (curve 2), for  $r = 3r_0$  (curve 3) and for  $r = 5r_0$  (curve 4). The shape of the graphs repeats the shape of the interaction force, but away from the source, a slight negative deflection  $P(t)$  appears, the amplitude decreases and the width of the disturbance increases. In point  $(0, r_0)$  at  $t = r_0/c_1 = 0.67$   $\mu$ s, longitudinal wave P will appear, in point  $(0, 3r_0)$  at  $t = r_0/c_1 = 2.0$   $\mu$ s and in point  $(0, 5r_0)$  at  $t = 5r_0/c_1 = 3.3$   $\mu$ s (see Fig. 8).

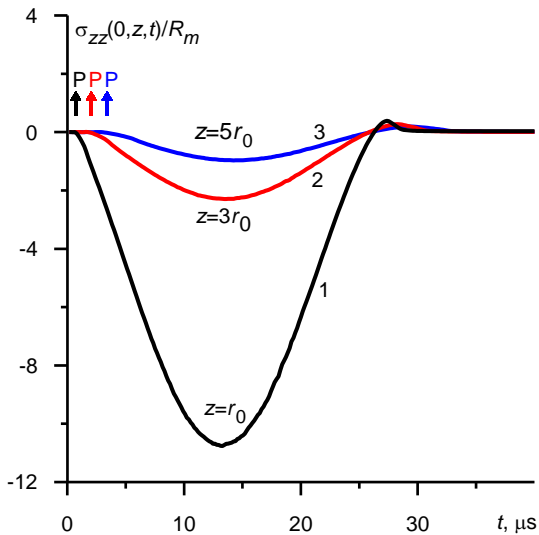


Fig. 9. Evolution of normal stress  $\sigma_{zz}(0, z, t)$  on the anvil axis due to load  $P(t)$  acting on the surface of a circle with a radius of the sample  $r_0$  for  $z = r_0$  (curve 1), for  $z = 3r_0$  (curve 2) and for  $z = 5r_0$  (curve 3)

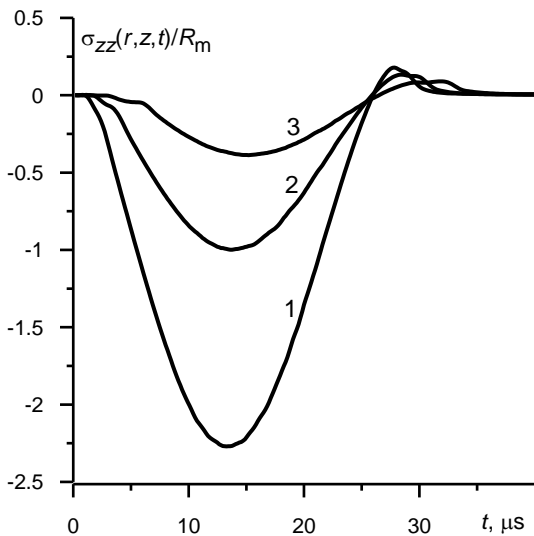


Fig. 10. Evolution of normal stress  $\sigma_{zz}(r, z, t)$  in the centre of the anvil due to the load  $P(t)$  acting on the surface of a circle with a radius of the sample  $r_0$  for  $z = r = 2r_0 / 2^{0.5}$  (curve 1), for  $z = r = 3r_0 / 2^{0.5}$  (curve 2) and for  $z = r = 5r_0 / 2^{0.5}$  (curve 3)

Fig. 9 shows dimensionless normal compressive stresses  $\sigma_{zz}(0, z, t)/R_m$  on the anvil axis due to load  $P(t)$  acting on the surface of a circle with a radius of the sample  $r_0$  for  $z = r_0$  (curve 1), for  $z = 3r_0$  (curve 2) and for  $z = 5r_0$  (curve 3). The amplitude of compressive stresses decreases. In point  $(0, r_0)$  at  $t = r_0/c_1 = 0.67 \mu s$ , longitudinal P stress wave will appear, in point  $(0, 3r_0)$  – at  $t = r_0/c_1 = 2.0 \mu s$ , and in point  $(0, 5r_0)$  – at  $t = 5r_0/c_1 = 3.3 \mu s$  (see Fig. 9).

Fig. 10 shows dimensionless normal stresses  $\sigma_{zz}(r, z, t)/R_m$  in the centre of the half-space on a cone at the same distances in point  $(2^{0.5}r_0, 2^{0.5}r_0)$  (curve 1), in point  $(3r_0/2^{0.5}, 3r_0/2^{0.5})$  (curve 2) and in point  $(5r_0/2^{0.5}, 5r_0/2^{0.5})$  (curve 3). The highest values of the compressive stress amplitudes decrease with increasing distance of the observation points from the disturbance site, but at the end of the stress disturbance, they change the sign into tensile stress.

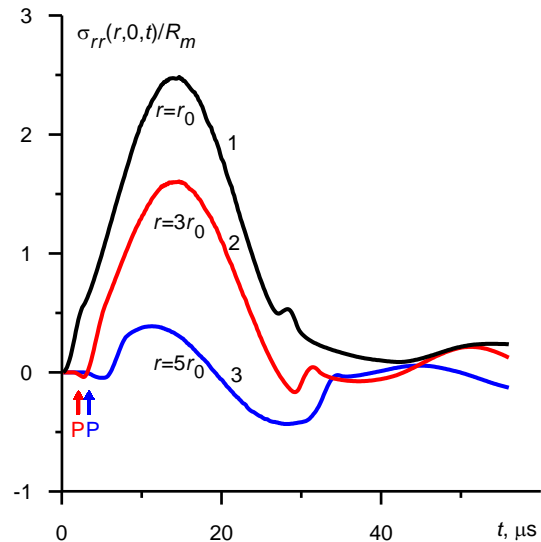


Fig. 11. Evolution of normal stress  $\sigma_{rr}(r, 0, t)$  on the surface of the anvil due to the load  $P(t)$  acting on the surface of the circle with the radius of the sample  $r_0$  for  $r = r_0$  (curve 1), for  $r = 3r_0$  (curve 2) and for  $r = 5r_0$  (curve 3)

Fig. 11 shows the time dependencies of normal stress  $\sigma_{rr}(r, 0, t)$  on the anvil surface due to load  $P(t)$  acting on the surface of a circle with a radius of the sample  $r_0$  for  $r = r_0$  (curve 1), for  $r = 3r_0$  (curve 2) and for  $r = 5r_0$  (curve 3). For example, let us consider an observation point  $(5r_0, 0)$  located on the anvil surface within 5 radiuses of the sample-anvil contact area. By the time  $t = (5r_0 - r_0)/c_1 = 2.67 \mu s$ , there are no disturbances. At  $t = 4r_0/c_1$ , there will be a disturbance with the speed of the longitudinal wave  $c_1$ . The arrows on the graphs correspond to the time of arrival at the appropriate observation points of the disturbance from the centre of the contact area of the sample with the anvil.

## 5. CONCLUSION

A mathematical model of the dynamics of the contact system of the test sample with the anvil (semi-elastic space) during their collision was developed. The proposed method of calculations using classical Laplace and Hankel transformations allows us to solve the problem for the spatial model of the body.

The proposed analysis enables the calculation of stresses and displacements in an elastic half-space, as well as the kinematics of the tested sample.

The original elements of the paper include the proposed general approach to solving the problem of contact dynamics. The presented approach consists in determining the impact force on the sample  $P(t)$  during the collision as a common solution to the problem for the tested sample and the problem for an elastic semi-space under the conditions of the assumptions of Hertz's theory. The resulting force  $P(t)$  allows the determination of displacements and stresses.

The performed calculations showed that during a sample collision with a half-space under the conditions under consideration, the contact force  $P(t)$  did not have a significant effect on the formation of visible waves: transverse (S) and Rayleigh (R) waves. This is because the rate of load change is not sufficient.

The obtained solution can be used to determine the dynamic strength limit of materials. The calculations made as part of the

paper showed more than threefold ( $1.6 \times 10^5$  N/S/R<sub>y</sub> = 3.18) increase of the dynamic yield point for steel and more than twofold ( $1.6 \times 10^5$  N/S/R<sub>m</sub> = 2.65) increase in dynamic tensile strength for steel to that determined in classical conditions. Corresponding values for a copper sample give a 14-fold ( $1.6 \times 10^5$  N/S/R<sub>m</sub> = 14.0) increase of the dynamic limit of tensile strength. Considering that the sample after reflection has the shape of a mushroom with a radius  $r_1 = 0.006$  m, we receive a sixfold ( $1.6 \times 10^5$  N/S<sub>1</sub>/R<sub>m</sub> = 6.2) increase of the dynamic tensile strength limit, where  $S_1 = \pi r_1^2$ .

The method proposed here can be useful for the dynamic analysis of issues such as the collision of a sample with a layered body [42].

## REFERENCES

- Taylor G. The use of flat-ended projectiles for determining dynamic yield stress. I. Theoretical considerations. Proc. R. Soc. London Ser. A. 1948;194:289–299.
- Whiffin AC. The use of flat-ended projectiles for determining dynamic yield stress. II. Tests on various metallic materials. Proc. R. Soc. London, Ser. A. 1948;194:300–322.
- Carrington WE, Gayler MLV. The use of flat-ended projectiles for determining dynamic yield stress. III. Changes in microstructure caused by deformation under impact at high-striking velocities. Proc. R. Soc. London, Ser. A. 1948;194:323–331.
- Włodarczyk E, Michałowski M. Penetration of metallic half-space by a rigid bullet. Problemy Techniki Uzbrojenia. 2002;31(82):93–102.
- Włodarczyk E, Sarzyński M. Analysis of dynamic parameters in a metal cylindrical rod striking a rigid target. Journal of Theoretical and Applied Mechanics. 2013; 51(4):847–857.
- Włodarczyk E, Sarzynski M. Strain energy method for determining dynamic yield stress in Taylor's test. Engineering Transactions. 2017; 65(3):499–511.
- Swierczewski M, Klasztorny M, Dziewulski P, Gotowicki P. Numerical modelling, simulation and validation of the SPS and PS systems under 6 kg TNT blast shock wave. Acta Mechanica et Automatica. 2012;6(3):77–87.
- Kil'chevskii NA. Dynamic Contact Compression of Two Bodies. Impact [in Russian]. Kiev: Naukova Dumka; 1976.
- Awrejcewicz J, Pyryev Yu. Nonsmooth Dynamics of Contacting Thermoelastic Bodies. New York: Springer Verlag; 2009.
- Saint-Venant BD. Sur le choc longitudinal de deux barres élastiques. J. de Math. (Liouville) Sér. 2. 1867;12:237–276. [http://portail.mathdoc.fr/JMPA/afficher\\_notice.php?id=JMPA\\_1867\\_2\\_12\\_A16\\_0](http://portail.mathdoc.fr/JMPA/afficher_notice.php?id=JMPA_1867_2_12_A16_0)
- Hertz H. Über die Berührung fester elastischer Körper [in German]. Journal für die reine und angewandte Mathematik. 1881;92:156–171.
- Boussinesq VJ. Application des potentiels à l'étude de l'équilibre et du mouvement des solides élastiques. Paris: Gauthier-Villars, Imprimeur-Libraire; 1885.
- Johnson KL. Contact mechanics. Cambridge: Cambridge University Press; 1985.
- Sears JE. On the longitudinal impact of metal rods with rounded ends. Proc. Cambridge Phil. Soc. 1908;14:257–286.
- Hunter SC. Energy absorbed by elastic waves during impact. J. Mech. Phys. Solids. 1957;5:162–171.
- Andersson M., Nilsson F. A perturbation method used for static contact and low velocity impact. Int. J. Impact Eng. 1995;16:759–775.
- Timoshenko SP, Young DH, Weaver WJr. Vibration Problems in Engineering. New York: Wiley. 1974.
- Popov SN. Impact of a rigid ball onto the surface of an elastic half-space. Soviet Applied Mechanics. 1990;26(3):250–256.
- Kubenko VD. Impact of blunted bodies on a liquid or elastic medium. International Applied Mechanics. 2004;40(11):1185–1225.
- Argatov II. Asymptotic modeling of the impact of a spherical indenter on an elastic half-space. International Journal of Solids and Structures. 2008;45:5035–5048.
- Argatov II, Fadin YA. Excitation of the Elastic Half-Space Surface by Normal Rebounding Impact of an Indenter. Journal of Friction and Wear. 2009;30(1):1–6.
- Argatov I, Jokinen M. Longitudinal elastic stress impulse induced by impact through a spring-dashpot system: Optimization and inverse. International Journal of Solids and Structures. 2013;50:3960–3966.
- Goldsmith W. Impact: The Theory and Physical Behavior of Colliding Solids. London: Edward Arnold Ltd.; 1960.
- Yang Y, Zeng Q, Wan L. Contact response analysis of vertical impact between elastic sphere and elastic half space. Shock Vib. 2018; vol. 2018: 1802174.
- Ruta P, Szydło A. Drop-weight test based identification of elastic half-space model parameters. Journal of Sound and Vibration. 2005;282:411–427.
- Qu A, James DL. On the impact of ground sound. Proceedings of the 22nd International Conference on Digital Audio Effects (DAFx-19), Birmingham, UK, September 2–6, 2019.2019:1–8.
- Lamb H. On the propagation of tremors over the surface of an elastic solid. Philos. Trans. R. Soc. London. Ser. A. 1904;203:1–42.
- Mooney HM. Some numerical solutions for Lamb's problem. Bulletin of the Seismological Society of America. 1974; 64 (2):473–491.
- Cagniard L. Réflexion et réfraction des ondes sismiques progressives, Gauthier-Villars. 1939.
- de Hoop AT. A modification of Cagniard's method for solving seismic pulse problems. Appl. Sci. Res. 1960; B8:349–356.
- Sánchez-Sesma FJ, Iturrarán-Viveros U, Kausel E. Garvin's generalized problem revisited. Soil Dyn. Earthq. Eng. 2013;47:4–15.
- Pak RYS, Bai X. Analytic resolution of time-domain half-space Green's functions for internal loads by a displacement potential-Laplace-Hankel-Cagniard transform method. Proc. R. Soc. A Math. Phys. Eng. Sci. 2020;476: 20190610.
- Pekeris CL. The seismic surface pulse. Proc. Natl. Acad. Sci. 1955; 41(7):469–480.
- Kausel E. Fundamental Solutions in Elastodynamics: a Compendium. Cambridge University Press; 2006.
- Kausel E. Lamb's problem at its simplest. Proceedings of the Royal Society A: Mathematical, Physical and Engineering Sciences. 2012;469:20120462.
- Emami M, Eskandari-Ghadi M. Lamb's problem: a brief history. Mathematics and Mechanics of Solids. 2019;25(3): 108128651988367
- Achenbach JD. Wave Propagation in Elastic Solids. New York: Elsevier. 1973.
- Nowacki W. Thermoelasticity. 2nd edn., PWN-Polish Scientific Publishers. 1986.
- Smetankina NV, Shupikov AN, Sotrikhin SYu, Yareshchenko VG. A Noncanonically Shape Laminated Plate Subjected to Impact Loading: Theory and Experiment. J. Appl. Mech. 2008;75(5): 051004.
- Awrejcewicz J, Pyryev Yu. The Saint-Venant principle and an impact load acting on an elastic half-space. Journal of Sound and Vibration. 2003;264(1):245–251.
- Panovko YaG. Introduction to the Theory of Mechanical Shock. Moscow: Nauka. 1977 [in Russian].
- Kulczycki-Zyhajło R, Kołodziejczyk W, Rogowski G. Selected issues of theory of elasticity for layered bodies. Acta Mechanica et Automatica. 2009;3(3):32–38.

Yuriy Pyryev:  <https://orcid.org/0000-0002-9824-2846>

Andrzej Penkul:  <https://orcid.org/0000-0001-9855-6610>

Leszek Cybula:  <https://orcid.org/0000-0002-8897-4779>